International Journal of Current Engineering and Technology

ISSN 2277 – 4106

Available at http://inpressco.com/category/ijcet

Research Article

Detection of Doctored Images

Uma Mudenagudi[a*], Lalitha M[b], Ananya U[c] , Harsh Holalad[c], Muktanidhi S D[d]

[a]Dept. of ECE, BVBCET, Hubli
[b]BVBCET, Hubli
[c]Juniper Networks, Bangalore
[d]PESIT, Bangalore

Abstract

In this paper we address the problem of detection of image doctoring. Doctoring is a process of altering or modifying the contents of an authentic image with varied motivations. We propose two frameworks to address the problem of detection of image doctoring: (i) bi-spectral analysis (ii) cor- relation pattern of the Point Spread Function (PSF) using iterative blind deconvolution (IBD). The most common types of the doctoring are splicing, cloning and re-touching. The detection of doctoring finds application in the area of digital forensic, law enforcement, medicine, security, military etc. In the first framework, using bispectral analysis, we capture the higher-order spatial content introduced due to the doctoring to detect the doctoring process. We use the deviation in the magnitude and the phase plots of bi-coherence to detect doc- toring. In the second framework we propose to use the cor- relation pattern of the estimated PSF in the detection process. In this case, we model the combined process of image cap- ture and doctoring as a linear filtering process. We use IBD to estimate the PSF of the filtering system. We demonstrate the proposed algorithms on different doctored images, which includes doctoring using splicing, cloning and re-touched im- ages.

Keywords: *Doctoring, bi-spectral, PSF, Blind decon- volution, Correlation.*

1. Introduction

In this paper we propose novel methods for the detection of doctored images. Doctoring is modifying an image beyond the direct methods of image edition and often inserts or deletes a key element. It leaves no visual clues, but some traces of the image doctoring operation in the image at the pixel level. The knowledge of whether an image is doctored, can play an essential role in every walks of life, from law en- forcement, military, medicine to the common man. This vital

information can be used to distinguish between an authentic image and a doctored image.The wide spread availability of multi-media data and the low-cost image editing tools, it is possible to project the falsehood as the authentic data for misleading people, for amusement or to stage an event that never happened.The wide spread availability of multi- media data and the low-cost image editing tools, it is possible to project the falsehood as the authentic data for mislead- ing people, for amusement or to stage an event that never happened. tools question the veracity of an image. Thus, detection of doctoring is essential because images are used as a source of evidence or to form decisions in the field of science, law, media etc. Typically, detection of doctoring can be classified into active and passive approaches. The active approaches require some kind of digital signature either during the manufacturing process of camera or some kind of added water marking after the image is captured. In most cases, images do not contain such information. Many researchers studying the field of image forensics, assume that when an image is doctored the image statistics are altered. The passive methods use these clues of alteration and check the authenticity of an image.

One of the methods in where authors use bi-coherence magnitude and phase for the detection of human speech splic- ing and the authors justify the approach saying that natural image from the camera has weak higher-order correlations, which results in low value of the bi-coherence feature. Some, where the authors use re sampling to detect doctoring and propose the Expectation-Maximization (EM) algorithm to an- alyze specific correlations brought into the re-sampled signal by the interpolation step. The output of the method is probability map containing periodic patterns, if the signal of inter- est has been re-sampled. The test fails when two images are re-sampled with same scale. Some, the authors deploy the bi- coherence magnitude and phase features to authenticate the image. The work is limited to image splicing detection. Some, the authors attempt to identify the doctored image, which are doctored by rotating, re-sampling, JPEG compressing etc using the Blind deconvolution method. However, all these methods are limited to a specific kind of doctoring process.

*Corresponding author: **Uma Mudenagudi**

In this paper we emphasize on three most commonly used doctoring processes namely- splicing, cloning and re-touching. We propose two frameworks for the iden-tification of doctored image. In the first framework we use the deviatio in the magnitude and phase response of the bi-coherence computed for the image. And also use Expectation-Maximization algorithm to detect the images that are not detected by the bi-coherence method. The second framework we propose to use the correlation pattern of the estimated PSF in the detection process. In total we make the following contribution:

- We use bi-coherence, which is higher order moment spectra to detect the presence of higher-order frequen-cies correlated with that of lower-order frequencies by computing the magnitude and phase.
- We use Expectation-Maximization algorithm to au-thenticate images that are not identified by the bi-spectral analysis.
- We also present a unified framework to address the problem of detection of doctoring using iterative blind deconvolution
- We demonstrate that correlation pattern of the estimated PSF can be used to detect doctoring: The deviation of the correlation patterns of the authentic and doctored set of images are analyzed based on the variance threshold of the correlation pattern.
- We compute the threshold for the variance of the correlation pattern of the estimated PSF, using variances of the correlation pattern of the estimated PSF for set of authentic and doctored images and then use this threshold to detect the doctoring without any prior information of the authentic image or the non-linear filter used to generate the doctored image.
- We implement these two frameworks on the three most common types of doctoring processes.

In Section 2, we provide details of the Bi-spectral framework and in Section 3, we demonstrate the deconvolution framework. The Section 4 provides information on the results and the discussions. We conclude the paper in Section 5.

2. Bi-spectral framework

In this section, we will give a brief introduction of bi-coherence and illustrate the way we estimate the 1-dimensional bi-coherence from a 2-dimensional image as given in . Bi- spectrum is defined as the Fourier transform of the third order moment of a signal x(t) and can be expressed as Equation 1 as the expected third-order or quadratic correlation of three harmonics from the Fourier transform of the signal, X (ω), at ω1 , ω2 and ω1 + ω2 .

$$B(\omega 1 , \omega 2) = E[X (\omega 1)X (\omega 2)X *(\omega 1 + \omega 2)] \quad (1)$$

Bispectrum is often used for detecting the existence of the quadratic correlation within a signal, as being applied in oceanography, EEG signal analysis, manufacturing, non-destructive structural fatigue detection and plasma physics applications.

We define the statistical quantity, bi-coherence, which is the base feature used in our detection of doctoring method presented in this section [10]. We denote the spatial variable and the frequency variable respectively as t and ω. A 1D spa- tial domain signal is represented by a lower-case letter, such as x(t), and its Fourier transform is represented by the corre- sponding upper-case letter, such as X (ω). The bi-coherence of a signal x(t) with a Fourier transform X (ω) is denoted by BX (ω1 , ω2). For complex algebra, we denote the magnitude of a complex variable z as |z|, its phase as φ(z), and its complex conjugate as z. Bicoherence is the normalized version of bispectrum and defined as in Equation 2.

$$B(\omega_1,\omega_2) = \frac{\frac{1}{N}\sum_i (X(\omega_1)X(\omega_2)X^*(\omega_1+\omega_2))}{\sqrt{\frac{1}{N}\sum_i (|X(\omega_1)X(\omega_2)|^2)\frac{1}{N}\sum_i (|X(\omega_1+\omega_2)|^2)}} \quad (2)$$

where |BX (ω1 , ω2)| ∈ [0, 1] and E(·) is the expected value of a random variable [tt4]. The expression for bicoherence. In Equation 2 is obtained by normalizing bispectrum with the Cauchy-Schwartz inequality upper bound on the magnitude of bispectrum. Hence, its absolute value is bounded between 0 and 1. The Cauchy-Schwartz upper bound is achieved when the harmonically related frequencies in the numerator is per- fectly phase coupled. In this case the magnitude of bicoher- ence is one and its phase, being Φ1 + Φ2 (Φ1 + Φ2), is zero [3]. In practice, for a 1D signal x(t), bicoherence is often esti- mated by sample averaging over the overlapping finite length segments sampled from the signal using Equation 3.

$$B(\omega_1,\omega_2) = \frac{\frac{1}{N}\sum_i (X(\omega_1)X(\omega_2)X^*(\omega_1+\omega_2))}{\sqrt{\frac{1}{N}\sum_i (|X(\omega_1)X(\omega_2)|^2)\frac{1}{N}\sum_i (|X(\omega_1+\omega_2)|^2)}} \quad (3)$$

In Equation 3, Signal is decomposed into N overlapping seg- ments, where a segment is denoted by Xi , with i = 1, ..., N Figure 1 shows how overlapping segments are obtained from a 1D slice of an image.

2.1. Bicoherence Features

For the limited data sample size, instead of computing 2-dimensional bicoherence features from an image, we compute

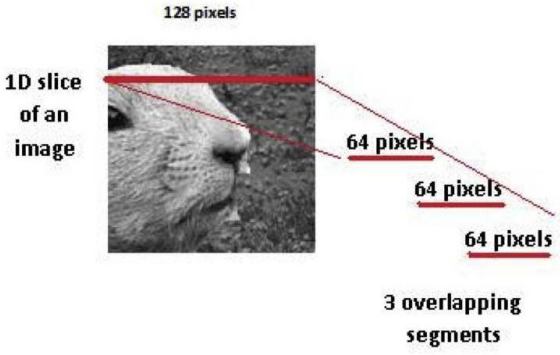

Fig. 1. Image capture process1D slices are extracted from a 2D image. A 1D slice is broken into overlapping segments for estimating bicoherence with Equation 2 (Image source: Columbia Image Splicing Detection Evaluation Dataset.

1-dimensional bicoherence magnitude and phase features from Nv vertical and Nh horizontal image slices of an image and then combined as in Equations 4 and 5. For the image blocks of 128 X 128 pixels in our data set, Nv = Nh =128.

$$fM = \sqrt{(\frac{1}{N_h}\sum_i M_i^h)^2 + (\frac{1}{N_v}\sum_i M_i^h)^2} \quad (4)$$

$$fP = \sqrt{(\frac{1}{N_h}\sum_i P_i^h)^2 + (\frac{1}{N_v}\sum_i P_i^h)^2} \quad (5)$$

In order to reduce the estimation variance, the 1-D bicoherence of an image slice is computed by segmenting 64 samples in length with an overlap of 32 samples with adjacent segments. Each segment of length 64 is multiplied with a Hanning window and then zero-padded from the end before computing 128-point DFT of the segment.

2.2. Bicoherence

In this section we explain the capability of bicoherence in detecting doctoring, in terms of its magnitude response and its phase entropy. We consider the doctoring operation as an addition of a bipolar signal to the source signal, and hence make a connection to the camera optical low-pass property [3]. Image doctoring induces a concentration of the bicoherence phase at $\pm 90^\circ$, instead of the $\pm 0^\circ$.

- *Bicoherence magnitude in detection of doctoring*

Given a pair of harmonics ω1 and ω2 , a non-linearity produces new harmonics ω1 + ω2 whose amplitude is correlated to ω 1 and ω2. As such correlations do not occur naturally, these correlation results in larger response in bicoherence magnitude.

- *Bicoherence phase in detection of doctoring*

If initial harmonics has phases Φ1 and Φ2 then the phases of newly introduced harmonics is Φ1 + Φ2 . It is seen that bicoherence phase for this pair of harmonics is zero. Such correlations do not occur naturally, the correlations results bicoherence phase towards zero. A phase bias towards π/2 also occurs due to the correla- tion of any harmonic ω1 with itself, as given by

$$B(\Phi 1, \Phi 2) = \Phi 1 + \Phi 1 - (2\Phi 1 - \pi/2) \quad (6)$$

Calculation of bicoherence indeed captures the higher-order correlation due to non-linearity of the doctored image. The sharp edges introduced by the image doctoring operation produce a unique magnitude response and phase in the bicoherence measurement computed from the image. Analysis shows that doctoring oper- ation results in an increase in bicoherence magnitude and phase concentration at $\pm 90^\circ$.

2.3. *Computation of Bicoherence Features*

We compute the phase histogram, the phase entropy and the magnitude response of the bicoherence of the image blocks. Given a 128 X 128-pixel image block in the dataset, we compute bicoherence individually on the horizontal and the vertical slices, each being a 128-pixel long 1D signal. The same computational procedure has been employed in. For each slice, bicoherence is estimated from three 64-pixel long overlapping segments where the overlap is 32-pixel long (Figure 1). When computing the discrete Fourier transform, the segments are multiplied with a Hanning window and extended to a length of 128 pixels by zero-padding, in order to reduce frequency leakage and obtain a better frequency resolution. The bicoherence phase histogram pφ , i=1, . . . ,24 for each slice is obtained by uniformly binning of the bicoherence phase (from -180◦ to 180◦) into 24 bins (bin width = 15◦). The phase histogram is then normalized so that it sums to 1. The overall phase histogram for an image block is ob- tained by averaging the phase histogram of the 1D slices. The magnitude response r_m and the phase entropy r_p of bicoher- ence is estimated as below:

$$r_m = \frac{1}{\Omega}\sum_{(\omega_1,\omega_2\in\Omega)} E(\omega_1,\omega_2), \qquad r_p = \sum_i p(\phi_i)log(p(\phi_i)) \quad (7)$$

r_m represents the averaged magnitude over all (ω1 , ω2) and r_p is the negative entropy of the bicoherence phase, where a higher rp represents a higher concentration of the bicoherence phase (i.e., less uniformly distributed). The overall magnitude response Rm and the overall phase entropy Rp of an image block is obtained by:

$$R_m = \frac{1}{128}\sum_{i=1}^{128} r_m^{hi} \qquad R_p = \frac{1}{128}\sum_{i=1}^{128} r_p^{hi} \quad (8)$$

where r^{hi}_m is the bicoherence magnitude response of the horizontal slices, indexed by i, while r^{hi}_m is for the phase

3. Deconvolution framework

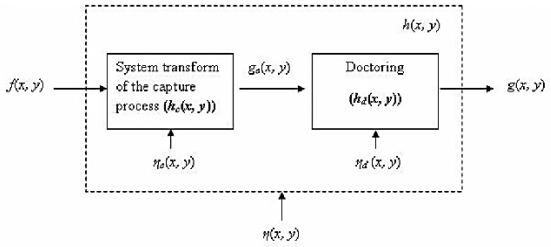

Fig. 2. Image capture process

To distinguish the authentic image from the doctored image, it is necessary to know the characteristics of the authentic image by the image capture process. We use Iterative Blind deconvolution to obtain the transfer function of the image capturing system.

The image formation model is given in Figure 2. The original image f (x, y) undergoes a transformation with hc (x, y), which is a system transform function and includes sensors and optical system. Consider the ηc (x, y) as the additive noise in the process as shown in the Figure 2. This generative model allows us to estimate the PSF and the estimates have high de- gree of correlations for the authentic images. The observed image gc (x, y) is given by

$$gc(x, y) = f(x, y) * hc(x, y) + \eta c(x, y), \quad (9)$$

where $*$ indicates the convolution operator. If the image is doctored, then the image gc (x, y) under-goes a doctoring process with the tamper filter hd (x, y) with additive noise ηd (x, y) as shown in the Figure 2 and the doctored image is given by

$$g(x, y) = gc(x, y) * hd(x, y) + \eta d(x, y). \quad (10)$$

The image formation process and doctoring process are considered as two systems connected in series and can be mod- eled as one process. The simplified doctoring process is shown as dotted lines in Figure 2. Using (9) in (10), we get

$$g(x, y) = f(x, y) * h(x, y) + \eta(x, y), \quad (11)$$

where $h(x, y) = hc(x, y) * hd(x, y)$ and $\eta(x, y) = \eta c(x, y) + \eta d(x, y)$.

In case of the authentic image and the absence of doctoring process, the PSF of the system is given by,

$$h(x, y) = hc(x, y). \quad (12)$$

This implies hd (x, y) = 1. Typically the estimates of hc (x, y) are space invariant for most of modern digital cameras and the estimates of PSF have large correlation pattern. Hence the correlation pattern (explained in Section 3) of the esti- mated PSF contains larger deviation for authentic images. However if the image is doctored, then hd (x, y) = 1 at some places. Then the estimates of h(x, y) may not contain high degree of correlation pattern. Therefore, we use the deviation of the correlation pattern in the estimates of h(x, y) to detect the given image is doctored or not. To detect the degree of correlation of the PSF, we use the iterative blind deconvolution algorithm proposed, to estimate simultaneously the original image f (x, y) and the PSF h(x, y).

3.1. Correlation of the PSF in Doctoring

In this section we present the relation between the correlation pattern in the estimated PSF of the authentic and doctored images. The frequency response of the actual filter and the estimated filters for the authentic and tampered images shown in Figure 3 (a) and (b) are shown in Figure 3 (c), (d) and (e) respectively. The distribution of the correlation pat tern for the rows of the estimated PSF is similar for authentic images and the distribution of the correlation pattern varies for the doctored image depending on the type of doctoring which affects the tampering filter. To compute the correlation pattern, we consider the frequency domain filter coefficients of the estimated PSF, Hb . The characteristics of the frequency domain filter coefficients, Hb for the authentic image are ob- served, which later serves as reference to detect the doctored images without having the knowledge of its authentic counter- part. The correlation pattern for the given image is computed

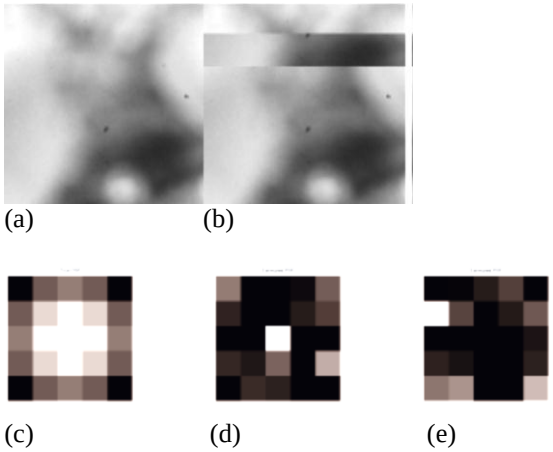

Fig. 3. Comparison of frequency response of the authentic and doctored image on synthetic data using 5 × 5 gaussian filter, (a) authentic image, (b) doctored image generated by splicing, (c) actual filter for an image, (d) estimated filter for authentic image, (e) estimated filter for tampered image.

by calculating the correlation between the current row and the preceding row iteratively for the entire set of the filter coeffi- cients Hb . The process of estimation of the correlation pattern is given in Algorithm 1.

Algorithm 1 Correlation pattern of $\widehat{H}$

Input: The estimated PSF coefficients, $\widehat{H}$
Output: Correlation pattern of $\widehat{H}$

for i=1 to number of rows **do**
  Correlation pattern (i)=Corr$(\widehat{H}(i,:), \widehat{H}(i+1,:))$
end for

The authentic image from the camera has a specific set of pixels that are statistically identical and spatially coherent, and have high degree of dependency to their neighboring pix- els due to the interpolation process as discussed in Section 3. Therefore, the filter coefficients of the authentic image pro- vides strong correlation to each of the neighboring pixels. As a result, the deviation is greater in the distribution of the cor- relation pattern which is demonstrated using synthetic images as shown in Figure 4(b) for the authentic image as shown in Figure 4(a). The synthetic doctored image (Figure 4 (c)) is generated by copy-pasting a patch of size 2 X 120 from the synthetic authentic image on to itself and filtering the gener- ated doctored image using rotationally symmetric Gaussian

low-pass filter of size 5 X 5 with standard deviation σ = 10. When the image is doctored, the dependency between the pix- els is altered, that disturbs the distribution of the correlation

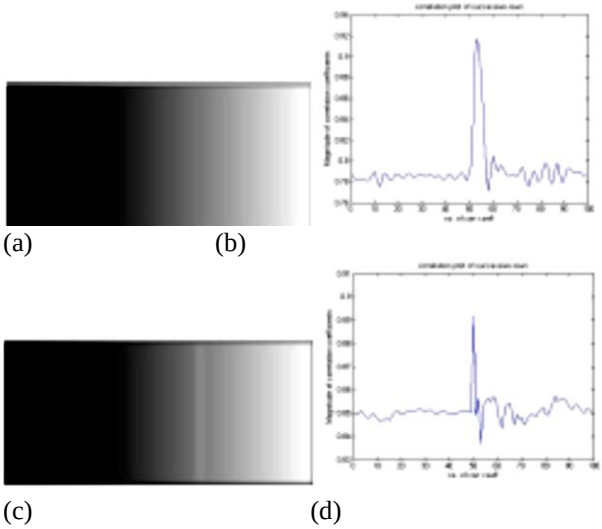

Fig. 4. Deviation in the correlation pattern for synthetically generated doctored image, (a) original image of size 255 × 120, (b) row-wise correlation pattern of PSF of authentic image shown in (a), (c) doctored image generated using splicing, (d) row-wise correlation pattern of PSF of the doc- tored image shown in (b).

pattern in the doctored image. Hence in the doctored images, the number of pixels contributing for a strong correlation pat- tern are less, which results in a small deviation in the corre- lation pattern as depicted in the Figure 4 (d) for the doctored image shown in Figure 4 (c).

4. Results and discussion

4.1. Bi-spectral Framework

We demonstrate the proposed method of detection of doctoring using different class of doctored images like spliced, cloned and re-touched images. In each case we consider a set of authentic and doctored images. We compute and com- pare the magnitude response and phase entropy for both the set of images and detect the doctored images based on the comparison of authentic and doctored set of images. The averaged magnitude and phase histogram for the authentic and doctored image blocks are as shown below. Note that the doctored block phase histogram is higher than the authentic one at $\pm 90^\circ$ but lower at 0°. In what follows we demonstrate the results for spliced, cloned and re-touched set of doctored images.

4.1.1. Splicing set

In this section we give the feasibility of the result on 120 spliced set of images, which contains 60 authentic images and corresponding 60 spliced images. We show the authentic im- age, its magnitude response and the phase plot, spliced images and its magnitude response and the phase plot are as shown in Figure 5 to 6.

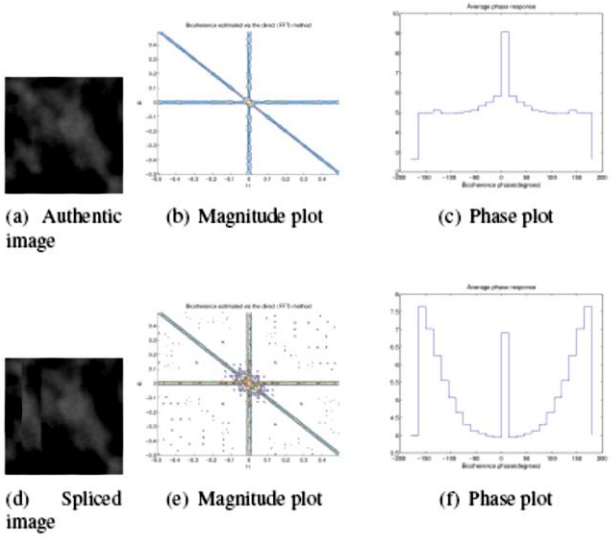

Fig. 5. Bicoherence magnitude and phase plots for spliced set of images (image source: Columbia Image Splicing Detection Evaluation Dataset)

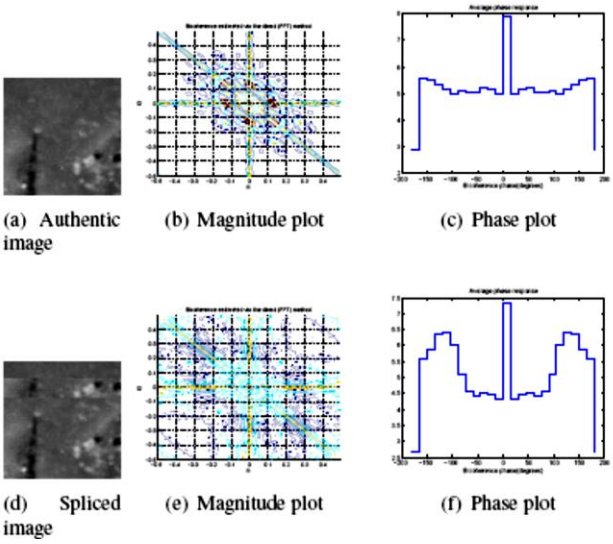

Fig. 6. Bicoherence magnitude and phase plots for spliced set of images (image source: Columbia Image Splicing Detection Evaluation Dataset)

4.1.2. Cloning set

We use 50 cloned of images in this section to test the for the authenticity of images, where 25 images are authentic and 25 are doctored. We show the authentic image, its magnitude response and the phase plot, cloned images and its magnitude response and the phase plot are as shown in Figure 7 and 8.

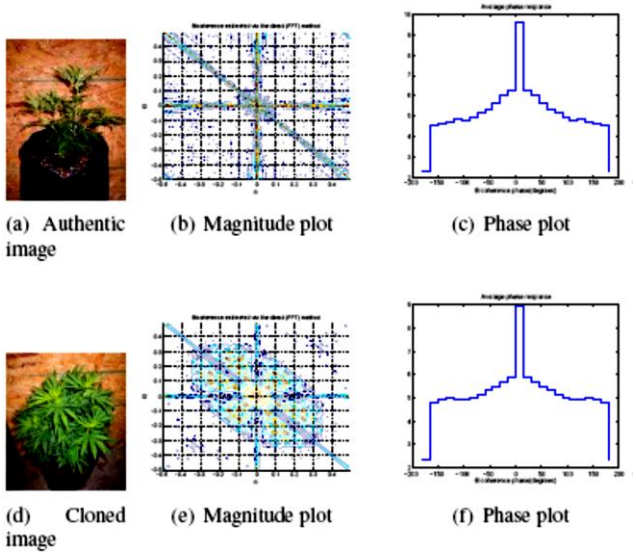

Fig. 7. Bicoherence magnitude and phase plots for cloned set of images (image source: WWW.Worth1000.com)

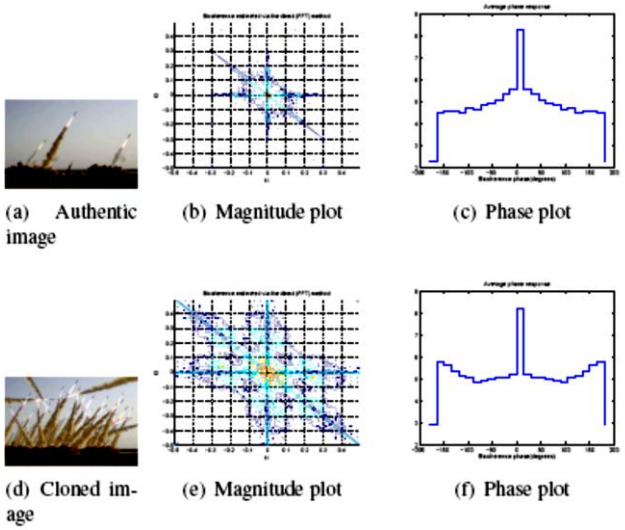

Fig. 8. Bicoherence magnitude and phase plots for cloned set of images (image source: WWW.Worth1000.com)

4.1.3. Retouched set

In this section we test the algorithm on 50 re-touched images with 25 authentic images and 25 re-touched images. We show the authentic image, its magnitude response and the phase plot, re-touched images and its magnitude response and the phase plot are as shown in Figure 9 and 10.

We compute the bicoherence magnitude response R_m and the bicoherence phase entropy R_p for the image blocks for different class of images and we find that the distributions of the Rm and Rp for the doctored images is greater than that of authentic images.

We observe that the method of detection of doctoring using bispectral analysis gives distinguishable results for the spliced image data set, than for the cloned and re-touched data sets. As discussed above, image splicing as a cut and paste of an image fragment onto another image without fur- ther post-processing, which introduces sharp edges and bicoherence detects such sharp edges introduced by the splicing operation which are not post-processed further. We observed that both Rm and Rp for the spliced image blocks are higher than those of the authentic image blocks in terms of distribution. A higher Rp represents a higher concentration of the bicoherence phase. We perform a baseline detection of the authentic and the spliced image blocks with Rm and Rp and obtained 60% ac- curacy, which is better than random guessing.

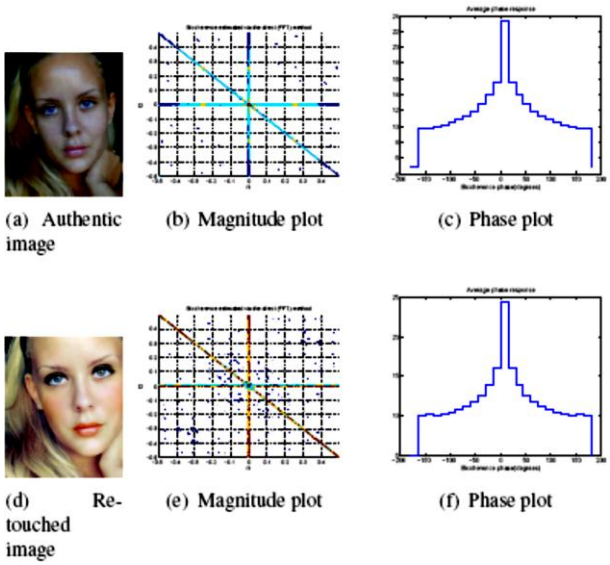

Fig. 9. Bicoherence magnitude and phase plots for re-touched set of images (image source: WWW.Worth1000.com)

We observe that bispectral analysis identifies spliced images, rather than the cloned and re-touched images. Hence we use Expectation-Maximization algorithm proposed in to detect cloned and re-touched set of images. In Expectation- Maximization algorithm, each samples belongs to one of the two models, samples correlated to neighbors and the other is, where samples not correlated. The algorithm runs iteratively in two steps:

· E-step: estimation of the probability of each pixel being correlated with its neighbor.

· M-step: estimation of the specific form of correlation between samples.

The results of detection of doctoring using Expectation- Maximization algorithm shows the discrete Fourier transform of the probability maps. Cloning and re-touching involves interpolation operation, where a sub-set of pixels which have undergone interpolation process has specific correlation intro-duced in to the interpolated image. The presence of periodic correlation gives the evidence of interpolation operation be- cause such correlations are unlikely to occur naturally. Hence we observe periodic pattern in the discrete Fourier transform of the probability maps, otherwise, we will get an

uniformity in the DFT mapping as shown in Figure 11 and 12. Detection of doctoring using Expectation-Maximization algorithm identifies cloned and retouched images.

We demonstrate the proposed algorithm using different class of doctored images like spliced, cloned and re-touched images. In each case we consider a set of authentic and doctored images and compute a desirable threshold in the correlation pattern. We use the computed threshold to detect the given image is doctored or not. In what follows we demonstrate the results for spliced, cloned and re-touched set of doctored images.

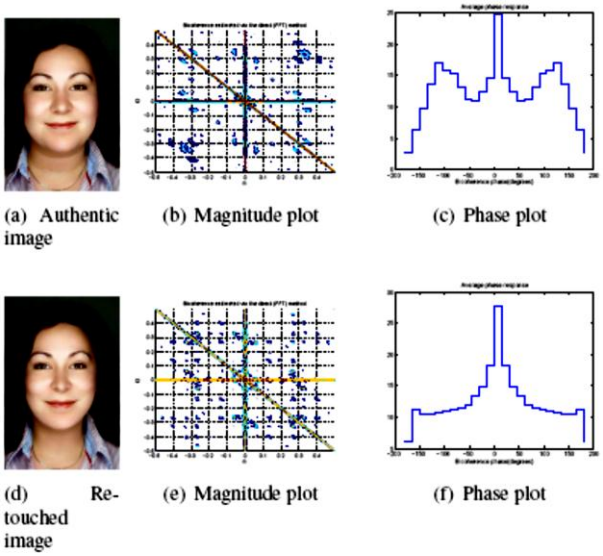

(a) Authentic image (b) Magnitude plot (c) Phase plot

(d) Re-touched image (e) Magnitude plot (f) Phase plot

Fig. 10. Bicoherence magnitude and phase plots for re-touched set of images (image source: WWW.Worth1000.com)

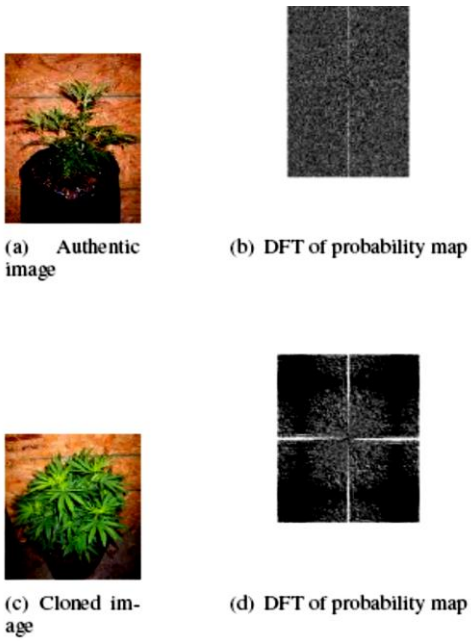

(a) Authentic image (b) DFT of probability map

(c) Cloned image (d) DFT of probability map

Fig. 11. Image and the DFT of the probability map of the image for cloned set of images (image source: WWW.Worth1000.com)

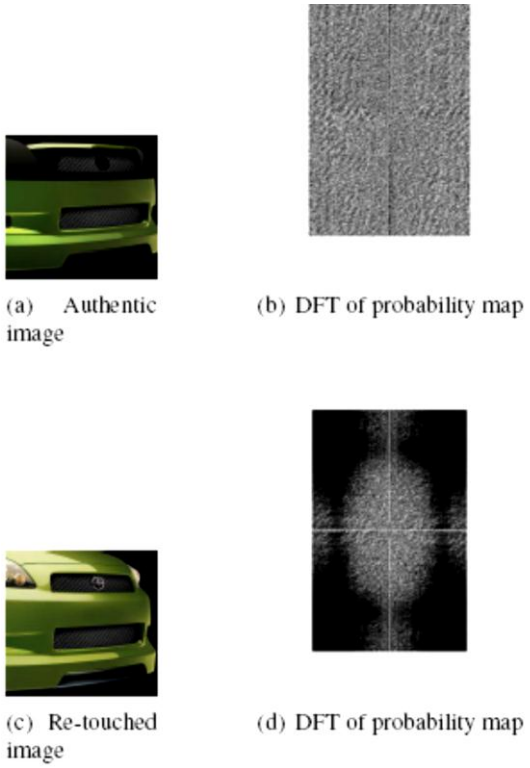

(a) Authentic image (b) DFT of probability map

(c) Re-touched image (d) DFT of probability map

Fig. 12. Image and the DFT of the probability map of the image for re-touched set of images (image source: WWW.Worth1000.com)

4.2. deconvolution Framework

4.2.1. Re-touching set

In this section we test the algorithm on 50 re-touched images with 25 authentic images and 25 re-touched images. Aver- age value of deviation for authentic images is 71.42 and for doctored images is 5. Hence we use a threshold of 5 for the detection of doctoring. We achieve an accuracy of 86% for the authentic images and 81% for the re-ouched images as demonstrated in Table 1 for a threshold of 10. We show the authentic image, its row-wise correlation, re-touched image and its row-wise correlation in Figure 13, 14 and 15 respec tively for variety of authentic and doctored images.

4.2.2. Cloning set

We use 50 cloned images to test the authenticity of images, where 25 images are authentic and 25 are doctored. We achieve an average deviation of 14.96 for authentic images and 5 for cloned doctored images. Hence we choose a threshold of 7 for the detection of the doctored images and obtain an accuracy of 84% for authentic images and 76% for doctored images as given in Table 1. We show the authentic image, its row-wise correlation pattern, the cloned doctored image and its row-wise correlation pattern in Figure 16, 17 and 18 respectively for variety of authentic and cloned doctored images.

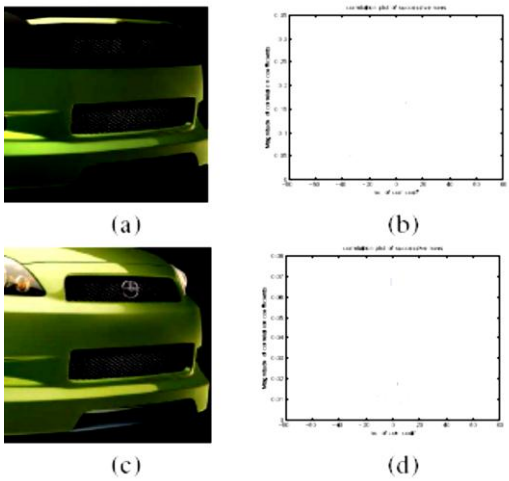

Fig. 13. Detection for re-toched image-1, (a) authentic image, (b) correlation pattern of (a) with variance=37, (c) doctored image (d) correlation pattern of (b) with variance=5 (image sourec: WWW.Worth1000.com).

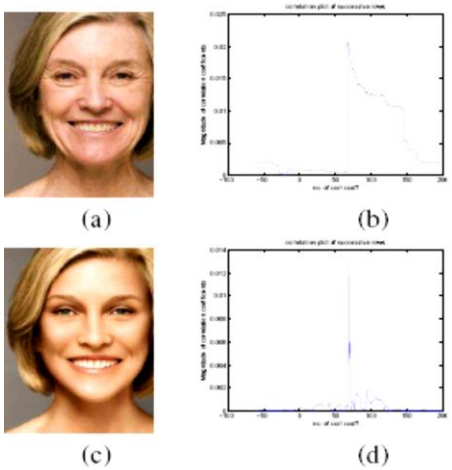

Fig. 14. Detection for re-touched image-2, (a) authentic im- age, (b) correlation pattern of (a) with variance=90, (c) doc- tored image, (d) correlation pattern for (b) with variance=2 (image sourec: WWW.Worth1000.com).

4.2.3. Splicing set

In this section we give the feasibility of the proposed detec- tion method using 120 images, which contains 60 authentic images and corresponding 60 spliced doctored images. We obtain an average value of deviation for authentic images as 22.58 and for doctored images as 10. Hence we use a threshold of 10 to detect spliced set of doctored images. We achieve an accuracy of 85% for authentic images and 55% for the doc tored images as shown in Table 1. We show the authentic im- age, its row-wise correlation, the spliced doctored image and its row-wise correlation in Figure 19, 20 and 21 respectively for variety of authentic and spliced doctored images.

From the results obtained for the images doctored using various doctoring methods, we notice that we get different threshold values for different class of doctored images which facilitates for the detection of doctoring.

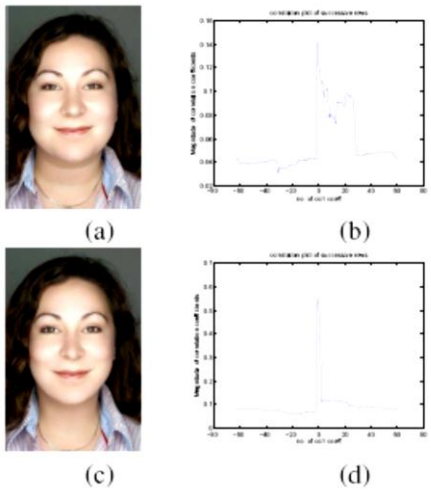

Fig. 15. Detection for re-toched image-3, (a) authentic im- age, (b) correlation pattern of (a) with variance=35, (c) doc- tored image, (d) correlation pattern of (b) with variance=3 (image sourec: WWW.Worth1000.com).

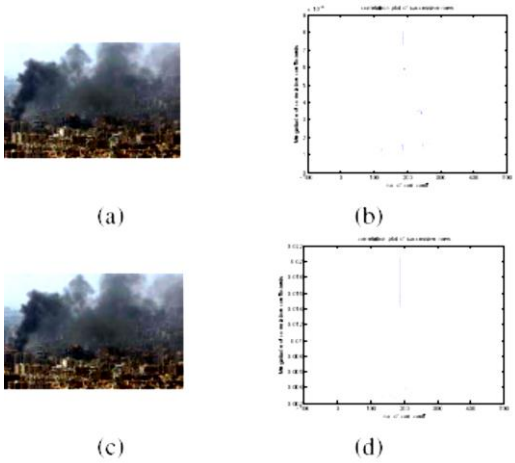

Fig. 16. Detection for cloned image-1, (a) authentic image, (b) correlation pattern of (a) with variance=60, (c) doctored image, (d) correlation pattern of (b) with variance=3 (image sourec: WWW.Worth1000.com).

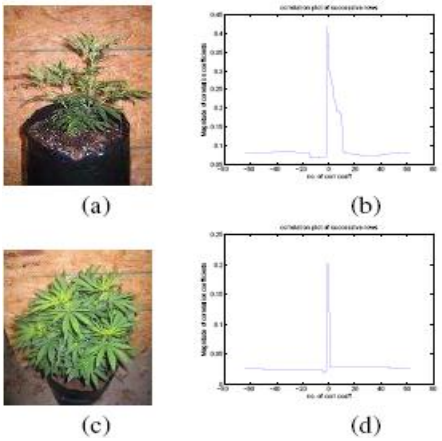

Fig. 17. Detection for cloned image-2, (a) authentic image, (b)correlation pattern of (a) with variance=17, (c) doctored image, (d) correlation pattern of (b) with variance=3 (image sourec: WWW.Worth1000.com).

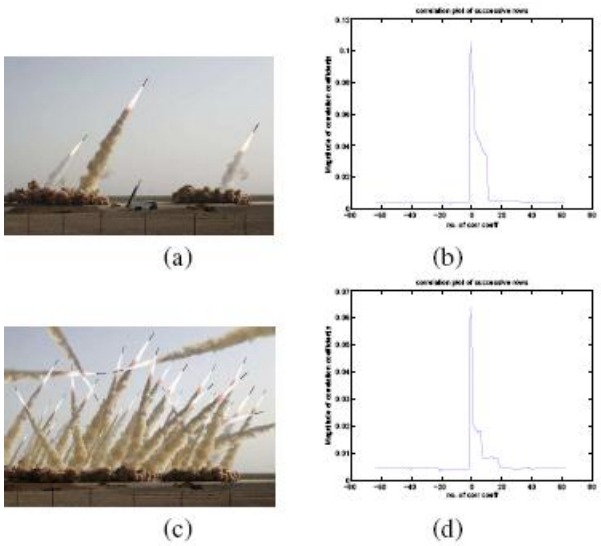

Fig. 18. Detection for cloned image-3, (a) authentic image, (b)correlation pattern of (a) with variance=15, (c) doctored image, (d) correlation pattern of (b) with variance=7 (image sourec: WWW.Worth1000.com).

5. Conclusion

In this paper, we have addressed the problem of detection of image doctoring using two frameworks:(i) bispectral analysis method and Expectation Maximization algorithm and (ii)iterative blind deconvolution. We have analyzed the detection of doctoring for spliced, cloned and re-touched doctored images. We have proposed the detection of doctoring using the bicoherence magnitude and phase response. We demonstrated the algorithm on different class of doctored images and on an average, obtained accuracy of 60% for all set of images. Bispectral analysis gives better detection for spliced images. Therefore Expectation-Maximization algorithm is used for the detection of cloned and re-touched image, which involve interpolation process to create good doctored images.

Table 1. Performance of the proposed detection method for different types of doctoring

Class of image	Image data set	Correct detection	False detection
Retouched	Authentic data set	86%	14%
	Doctored data set	81%	19%
Cloned	Authentic data set	84%	16%
	Doctored data set	76%	24%
Spliced	Authentic data set	85%	15%
	Doctored data set	55%	45%

In the second framework, we have proposed the detection of doctoring using the correlation patterns of the estimated PSF. We have presented a unified framework which uses a generative model of the imaging process and addresses the problem of detection of image doctoring. We have combined image capture and doctoring process into single framework. We demonstrated the algorithm on different class of doctored images and on an average, obtained accuracy of 74% for all sets images.

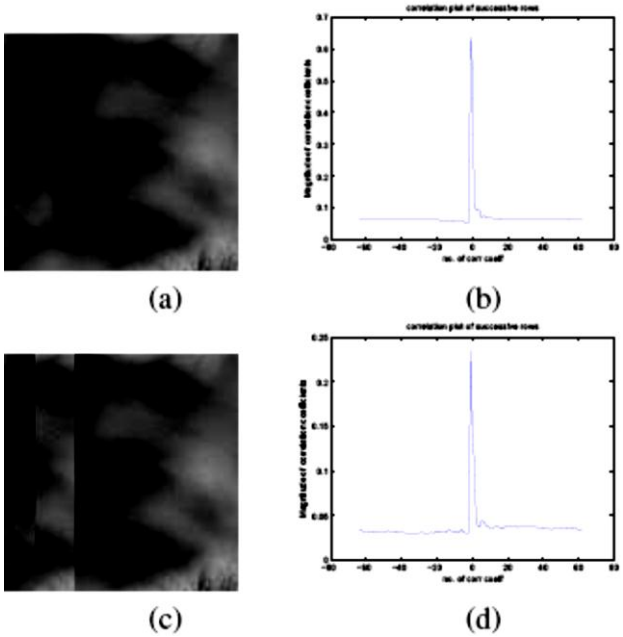

Fig. 19. Detection for spliced image-1, (a) authentic image, (b)correlation pattern of (a) with variance=7, (c) doctored image, (d) correlation pattern of (b) with variance=6 (image source: Columbia Image Splicing Detection Evalu- ation Dataset).

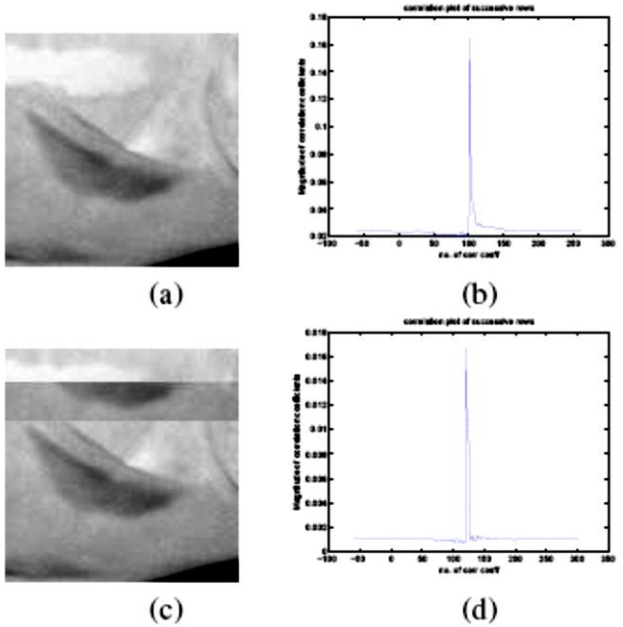

Fig. 20. Detection for spliced image-2, (a) authentic image, (b)correlation pattern of (a) with variance=5, (c) doctored im- age (d) correlation pattern with variance=2 (image source: Columbia Image Splicing Detection Evaluation Dataset).

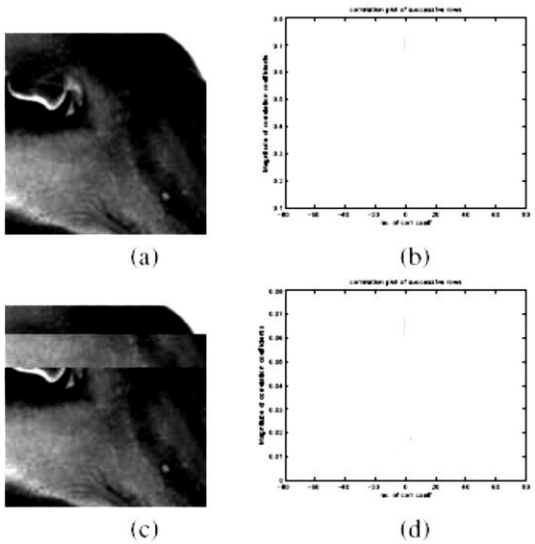

Fig. 21. Detection for spliced image-3, (a) authentic image, (b)correlation pattern of (a) with variance=8, (c) doctored im- age (d) correlation pattern with variance=4 (image source: Columbia Image Splicing Detection Evaluation Dataset).

References

Kalyan Sunkavalli, Micah K. Johnson, Wojciech Ma- tusik, and Hanspeter Pfister (2010), Multi-scale image harmo nization, *ACM Transactions on Graphics* (Proc. ACM SIGGRAPH), vol. 29, no. 4, pp. 125:1–125:10.

M.K. Johnson, K. Dale, S. Avidan, H. Pfister, W.T. Free- man, and W. Matusik (2011), Cg2real, *IEEE Transactions on Visualization and Computer Graphics*.

Jiri Fridrich (1998), Image watermarking for tamper detec- tion, in *International Conference on Image Processing*,pp. 404–408.

H. Farid (1999), Detecting digital forgeries using bispectral analysis, Tech. Rep. AIM-1657, AI Lab, *Massachusetts Institute of Technology*.

A.C. Popescu and H. Farid (2005), Exposing digital forgeries by detecting traces of re-sampling, *IEEE Transactions on Signal Processing*, vol. 53, no. 2, pp. 758–767.

Tian-Tsong Ng and Shih-Fu Chang (June 2004), Blind detection of digital photomontage using higher order statistics, Tech. Rep., *Columbia University*.

Ashwin Swaminathan, Min Wu, and K. J. Ray Liu (2006), Im- age tampering identification using blind deconvolution, in Proc. *IEEE ICIP*,pp. 2311–2314.

Hany Farid, Digital doctoring: How to tell the real from the fake, ICASSP '09 Proceedings of the 2009

IEEE International Conference on Acoustics, Speech and Signal Processing, vol. 3, no. 4, pp. Pages 162–166, 2006.

Tian Tsong Ng (2007), Statistical and geometric methods for passive-blind image forensics,

T.-T. Ng and S.-F. Chang (Oct 2004), A Model for Image Splicing,

Tian-Tsong Ng and Shih-Fu Chang (June 2004), A data set of authentic and spliced image blocks, Tech. Rep., Columbia University.

Uma Mudenagudi, Subhashis Banerjee, and Prem Kumar Kalra (2011), Space-time super-resolution using graph- cut optimization, *IEEE Trans. Pattern Anal. Mach. In- tell.*, vol. 33, no. 5, pp. 995–1008.

G. R. Ayers and J. C. Dainty (1998), Iterative blind deconvolu- tion method and its applications, *Optimization Letters.*